JOURNAL OF AGRICULTURAL AND FOOD CHEMISTRY
ARTICLE

J. Agric. Food Chem. **2010,** *58,* 967–974 **967**
DOI:10.1021/jf902349q

Small-Angle X-ray Scattering Study of the Effect of pH and Salts on 11S Soy Glycinin in the Freeze-Dried Powder and Solution States

Anna Sokolova,*[,†,‡] Catherine S. Kealley,[†,‡,§] Tracey Hanley,[†] Agata Rekas,[∥] and Elliot P. Gilbert*[,†]

[†]Bragg Institute, Australian Nuclear Science and Technology Organisation, PMB 1, Menai, NSW 2234, Australia, [‡]Food Futures Flagship, P.O. Box 52, North Ryde, NSW 2113, Australia, and [∥]National Deuteration Facility, Australian Nuclear Science and Technology Organisation, PMB 1, Menai, NSW 2234, Australia. [§]Current address: Institute for Nanoscale Technology, University of Technology, Sydney, P.O. Box 123, Broadway, NSW 2007, Australia.

The nanostructures from powders of native protein, glycinin, and corresponding solutions from which the powders have been formed, have been studied as a function of pH and 1 M salts using small-angle X-ray scattering. All powders showed Porod scattering with the exception of that prepared from the solution close to pI which displayed fractal behavior. Well-defined Bragg peaks in the powder scattering at pH 5, pH 7, and 1 M NaCl indicate the presence of long-range order. The scattering from solutions at pH 7, pH 9, and 1 M NaCl can be described well on the basis of particles derived from the known atomic structures of homohexameric glycinin. Extreme acidic (pH 2) and basic (pH 11) environments lead to the partial denaturation of glycinin. Decreasing the pH to 2 initiates dissociation of the hexameric structure, while increasing the pH to 11, as well as the presence of 1 M NaSCN, results in the formation of large unimodal particles. This is reflected by "featureless" SAXS patterns for both powders and solutions.

KEYWORDS: 11S; glycinin; SAXS; protein; freeze-dried; pH; Hofmeister; powder

1. INTRODUCTION

Dried protein powders find wide application in food manufacturing, not only for their nutritional value but also for their properties, as thickeners, gelling agents, and film-forming and texturing agents in products as diverse as drinks, sauces, spreads, ice cream, baked goods, and snacks. One such protein is glycinin, the principal storage protein in soy bean, that acts as a sink for nitrogen, sulfur, and carbon. It accounts for more than 40% of the total soybean protein and can be easily fractionated. Glycinin contains 3−4 times more methionine and cysteine per unit protein when compared with other storage proteins of soybean and is commonly used as an ingredient in vegetarian foods as the protein contains all essential amino acids for human nutrition (*1*).

Glycinin is a heterogeneous protein with a polymorphic subunit composition, which varies among different cultivars. The currently accepted model of native glycinin is a hexamer consisting of two layers of trimers (*2*). Each trimer is composed of three acidic (A) (31−45 kDa) and three basic (B) (18−20 kDa) polypeptides paired to form subunits (58−69 kDa) and held together by disulfide and hydrogen bonds (*1*, *3*−*5*). Five major subunits have been characterized, namely, A1aB2, A1bB1b, A2B1a, A3B4, and A5A4B3. The crystal structure of the A1aB1b subunit forms a homotrimer in solution (*6*), and the glycinin A3B4 subunit from a soybean mutant line associates into the homohexamer (*7*) [**Figure 1**, visualized using Rasmol (http://www.umass.edu/microbio/rasmol)]. Both of these structures were recently determined by X-ray analysis. These studies also revealed that the glycinin subunits are folded into two jellyroll β-barrel domains and two α-helix domains that form a cavity (a cup, from which the name cupin for the structural superfamily was derived) in addition to a binding site for hydrophobic ligands.

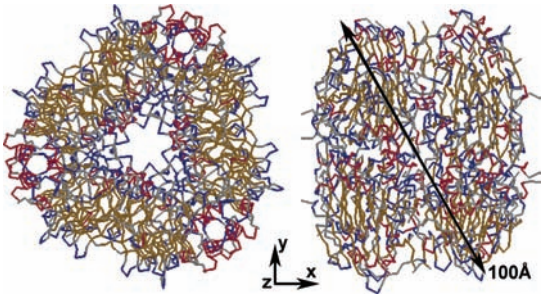

Figure 1. Homohexamer A3B4 (Protein Data Bank entry 1od5). The right panel shows the left view rotated by 90° around the OY axis.

According to Lakemond et al. (*8*, *9*), a pH value of 7.6 and an ionic strength of 0.5 M NaCl provide the most stable form of glycinin in solution. Under these conditions, the protein has a hexameric form with a molecular mass of 360 kDa, a maximum

*To whom correspondence should be addressed. A.S.: e-mail, anna.sokolova@ansto.gov.au; phone, (+61) 2 9717 7288; fax, (+61) 2 9717 3606. E.P.G.: e-mail, elliot.gilbert@ansto.gov.au; phone, (+61) 2 9717 9470; fax, (+61) 2 9717 3606.

Published on Web 12/21/2009

dimension equal to 100 Å, and a sedimentation coefficient of 11S, consistent with the findings of Badley et al. (*2*) three decades earlier. It has also been shown that a decrease in pH leads to dissociation of glycinin into trimers and then into individual subunits and finally breakage into 12 separated polypeptides. Kim et al. (*10*) studied the influence of pH and heating on glycinin structure using circular dichroism (CD) and differential scattering calorimetry (DSC) techniques. Aggregation of the polypeptide chains occurs in solutions with a pH close to the glycinin isoelectric point (pI) of 5.1.

Ultracentrifugal and CD measurements have been taken to determine the effects of pH, ionic strength, and storage time on the behavior of the 11S protein in acidic solutions (*11*). The data suggest that 11S glycinin undergoes acid-induced conformational changes for two reasons: (i) dissociation of the proteins into subunits due to electrostatic repulsion of charged groups and (ii) destruction of the gross structures and unfolding of the polypeptide chains. It has therefore been proposed that it is impossible to dissociate glycinin into its constituent subunits without unfolding of its internal structure. Information about the mechanism and extent of denaturation has also been obtained by observing changes in the secondary structure using CD. Acidic denaturation of glycinin starts at pH 3.75 and reaches a maximum at pH 2, whereas alkali denaturation starts at pH 10 and proceeds more rapidly at pH >11.4 (*11*). CD generates profiles of glycinin that are not significantly altered over a wide range of pH values, even under acidic and basic conditions, but increasing the salt concentration at pH 8.0 results in an increase in the percentage of α-helix. A pH between 4.0 and 5.5, i.e., around the pI of glycinin, introduces the appearance of turbid aggregates without any significant presence of secondary structure elements such as α-helices and *β*-sheets (*10*). DSC shows that, for pH values of >11.5 and <3.0, the typical endothermic peak of glycinin disappears; this is considered to be indicative of complete denaturation of the protein (*10*). The authors (*10*) explain the discrepancy between CD and DSC data by the possible presence of untwisted α-helical regions even in the denatured protein.

Studies of the influence of ions in solution on protein structure began almost one and one-half centuries ago, leading to the development of the Hofmeister series (*12*). The latter represents a list of ions ordered by their ability to change the solubility of proteins and the stability of their secondary and tertiary structure. It was later discovered that the ability of ions to change the structure of water occurs in the same order; it was therefore believed that such water structural changes caused a variation in protein solubility. Thus, ions were grouped according to their supposed influence on water structure into the following groups: chaotropes ("water structure breakers", for example, Cl^-, Br^-, I^-, and SCN^-) and kosmotropes ("water structure makers", such as $H_2PO_4^-$ and $S_2O_3^{2-}$). However, there is now an extensive debate about whether the ions truly impart a water structure-breaking or -making effect on protein solutions (*13*−*16*). Indeed, more recent experimental data provided evidence that changes in bulk water structure caused by added salts cannot explain the effects of specific ions. Instead, Hofmeister phenomena can be understood in terms of direct interactions between the ions and the macromolecules (*17*). In this sense, Hofmeister ions salt-out nonpolar groups and salt-in the peptide group. A nonspecific salting-in interaction is known to occur between simple ions and dipolar molecules; this depends on their ionic strength and not on their position in the Hofmeister series.

One should be careful in predicting the precise influence of particular ions on protein stability. Ions interact with proteins in a variety of ways, and often these interactions are specific to the protein and to the particular conditions employed (pH, temperature, and salt concentration) (*18*). For example, NaCl at certain concentrations is a protein structure stabilizer, as it stabilizes hydrophobic interactions (*19*). On the other hand, the relative destabilizing effects of salts on the properties of proteins follow the lyotropic series for anions: $Cl^- < Br^- < SCN^-$ (*12*). Low-concentration neutral salts affect electrostatic interactions between charged groups in a protein, whereas at higher concentrations, neutral salts also have ion-specific effects on hydrophobic interactions (*20*).

Protein function depends critically on its structure, and this is affected by its microenvironment, such as pH and ionic strength (*21*). This study focuses on the influence of several chaotropic ions, namely, Cl^-, Br^-, I^-, SCN^-, and pH on the protein stability of 11S glycinin. In addition, this study has investigated the nanostructure of glycinin powders at a moisture content of 6% as a function of pH and ionic strength. The latter complements recent studies of powders at constant pH and as a function of moisture content without the addition of salts (*22*). Bragg peaks are observed in the small-angle X-ray (SAXS) and neutron scattering, indicating the long-range order of glycinin molecules within the crystals and in which the unit cell undergoes a small increase with increasing moisture content from 5 to 21%. The structure of this native material composed of multimeric subunits was compared with the reported structure of a mutant glycinin composed of homohexameric subunits (*7*). The challenge in this work is to relate the structure of native glycinin in the final powdered form to the structure of the protein in the solution from which the powder has been produced by being freeze-dried and to observe the influence of external conditions on both solid and solvated structures. An understanding of this relationship is relevant to the food industry where commonly, for ease of transport and storage, proteins are typically purified, freeze-dried from solution, and subsequently used by manufacturers in the form of purified, dried powders.

2. MATERIALS AND METHODS

2.1. Sample Preparation. Soy glycinin 11S was extracted following a modified protocol of Bogracheva et al. (*23*) from defatted soy flour initially obtained from Archer Daniels Midland Co. (ADM). Purified glycinin was dissolved in 10 mM phosphate buffer (pH 7) to generate a concentration of 10 mg/mL. Further values of pH were adjusted with HCl or NaOH to pH 2, 5, 7, 9, and 11. Sodium chloride (NaCl), sodium bromide (NaBr), sodium iodide (NaI), and sodium thiocyanate (NaSCN) were used to prepare powders and solutions with different anion contents through the addition of the appropriate amount of powdered salts to a pH 7 solution to yield a concentration of 1 M. Once stabilized, either liquid aliquots were taken and stored at 4 °C or the solutions were freeze-dried. All final powders were hydrated to 6% moisture content by being placed in sealed containers with silica gel and conditioned for several weeks in a desiccator prior to the determination of the weight of water in the material to the weight of hydrated material as a percentage.

The purities of glycinin solutions were checked by polyacrylamide gel electrophoresis. Protein concentrations were measured immediately prior to SAXS experiments using protein absorption measurements at a wavelength of 280 nm on NanoDrop-1000 (at the European Molecular Biology Laboratory c/o DESY) or Cary 50 UV−vis (at the Bragg Institute, ANSTO) spectrophotometers. The extinction coefficient for native 11S glycinin was approximated on the basis of extinction coefficients provided by the ExPasy portal (*24*) for the primary structures of all five subunits. The stability of samples was checked by dynamic light scattering (DLS).

Glycinin has a strong tendency to aggregate; consequently, only solutions with relatively low concentrations were suitable for SAXS study. Thus, the following samples were prepared: 2.1 and 3.5 mg/mL for pH 2 solutions, 1.3 mg/mL for pH 7 solutions, 0.85 and 3.0 mg/mL for pH 9 solutions, 2.5 and 4.1 mg/mL for pH 11 solutions, 2.7 mg/mL for a 1 M NaCl solution, 2.7 and 5.1 mg/mL for a 1 M NaBr solution, and 3.0 and

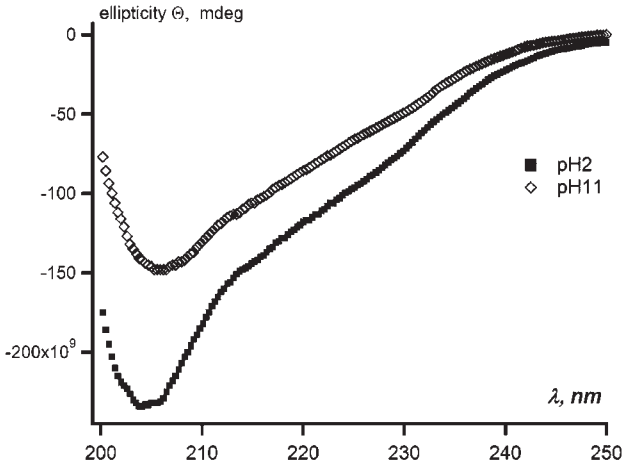

Figure 2. CD data for solutions at pH 2 (■) and pH 11 (◇).

4.4 mg/mL for a 1 M NaSCN solution. To check monodispersity, all samples listed above were studied by DLS at unchanged concentrations.

Monodisperse solutions of the A5A4B3 subunit were prepared following the protocol of Nagano et al. (*28*) in the Laboratory of Food Quality Design and Development at the Graduate School of Agriculture at Kyoto University (Kyoto, Japan) and kindly supplied by S. Utsumi. To obtain suitable samples, A5A4B3 solutions were dialyzed overnight against 10 mM phosphate buffer with 0.4 M NaCl, after which protein concentrations were checked by measurements of UV absorption at 280 nm and the level of monodispersity was verified by DLS.

Semi-native SDS electrophoresis indicated that all glycinin solutions were not 100% monodisperse; a small quantity of protein contaminants was present. This is in agreement with our previous studies that indicated that the purification protocol used yields a protein purity of 96.3% (*22*).

2.2. Dynamic Light Scattering. Prior to solution-based SAXS measurements, the monodispersity of the solutions was checked with dynamic light scattering on a DynaPro Titan (Wyatt). The results are mass and intensity distributions as a function of the hydrodynamic radius (R_h) of the particles. Most of the obtained dependencies show that each solution contains one major species and a small quantity of larger particles. The average hydrodynamic radius of those species lies in the range between 40 and 140 Å. Such a broad distribution reflects a tendency for large oligomers to be formed with an increase in pH and the presence of salts. Estimated values for the radii of gyration of the A1aB1b trimer and A3B4 hexamer [with HYDRO (*25*−*27*)] are equal to 40−50 Å. Since the anisometry and the maximum size of both the trimer and hexamer are very close, the hydrodynamic parameters for both oligomers are similar.

2.3. Circular Dichroism. To supplement scattering information about quaternary shape changes at dramatically low or high pH values, CD spectroscopy was used to investigate changes in secondary structure. Two glycinin solutions at pH 2 and 11 [the concentration of each was 0.2 mg/mL (**Figure 2**)] in Tris buffer (pH 8.0) were analyzed on a Jasco J-815 CD spectrometer using a 0.2 cm path length quartz cuvette (Starna, Sydney, Australia) at 20 °C. Data were collected at a wavelength range from 190 to 250 nm with a wavelength step of 0.1 nm, a response time of 4 s and a scan rate of 200 nm/min. Each spectrum was an average of four scans with a baseline spectrum subtracted. Online software DICHROWEB (*29*) from the Web site http://dichroweb.cryst.bbk.ac.uk was used for data analysis.

2.4. Small-Angle X-ray Scattering (SAXS). *2.4.1. SAXS from Solutions*. Synchrotron radiation X-ray scattering data from glycinin solutions (at pH 2, 7, 9, and 11 and in the presence of 1 M NaCl, 1 M NaBr, and 1 M NaSCN) were collected using standard procedures on the X33 camera of the EMBL on storage ring DORIS III of the Deutsches Elektronen Synchrotron (DESY) equipped with a 2D Photon counting Pilatus 500k detector. The beam was focused onto the detector placed 2.7 m from the 50 μL sample cell. The covered range of s is from 0.005 to 0.52 Å^{-1}, where s is the modulus of the scattering vector defined as $(4\pi/\lambda)$ sin θ, using a wavelength, λ, of 1.5 Å and 2θ is the scattering angle.

The data were processed using standard procedures within PRIMUS (*30*) and further analyzed with ATSAS (*31*). To check for radiation damage and aggregation during the SAXS experiment, data were collected in four successive 30 s frames. The absence of radiation damage was confirmed.

Small-angle X-ray scattering from the A5A4B3 subunit solution was collected on a Bruker Nanostar SAXS camera equipped with a Vantec-2000 detector, with pinhole collimation for point focus geometry. The instrument source is a copper rotating anode operating at 45 kV and 110 mA, fitted with cross coupled Göbel mirrors, resulting in a Cu Kα radiation wavelength 1.54 Å. The SAXS camera was fitted with a Hi-star 2D detector with an effective pixel size of 100 μm. Protein and buffer solutions were measured using a reusable 2 mm quartz capillary. The optics and the sample chamber were under vacuum to minimize air scatter. The sample−detector distance used was 112 cm, covering a range of s from 0.011 to 0.21 Å^{-1}. Each data set was collected over the course of 1 h. Possible protein damage and aggregation were checked by comparison of short-time data set prior to, and following, each 1 h run. No changes in scattering with time were observed.

The forward scattering $I(0)$, distance distribution functions $p(r)$, and radii of gyration R_g were evaluated with the indirect transform package GNOM (*32*, *33*). The scattering intensities from reported atomic positions were computed using CRYSOL (*34*). The similarity between two aligned three-dimensional (3D) structures is described by the normal spatial discrepancy (NSD) calculated with SUPCOMB (*35*). For every atom in the first structure, the minimum value among the distances between this atom and all atoms in the second structure is found, and this is repeated for all atoms in the first structure. These distances are summed and normalized against the average distances between the neighboring points for the two models. From alignment of the axes of inertia, the algorithm minimizes the NSD with the final value providing a quantitative estimate of the similarity between the objects. An NSD value of ≤1 indicates that the two models are structurally identical.

2.4.2. SAXS from Powders. Native glycinin powders, equilibrated to 6% moisture content, prepared from the solutions described above were loaded into 2 mm quartz capillaries that were sealed for the collection of SAXS data. SAXS measurements were performed on a Bruker Nanostar SAXS camera (as described above). A sample−detector distance of 250 mm was used, giving an s range of 0.05−0.8 Å^{-1}. Scattering files were normalized by transmission. Background was subtracted, and data were then radially averaged using the Nika (*36*) program in Igor from Wavemetrics (www.wavemetrics.com/products/igorpro/igorpro.htm).

3. RESULTS AND DISCUSSION

SAXS data from powders and solutions of glycinin prepared at various pH values (2, 5, 7, 9, and 11) and salt solutions are shown in **Figure 3**.

3.1. Effect of pH and Salts on Glycinin Structure in Solution. *3.1.1. Overall Parameters Obtained from Scattering Data*. Solution small-angle scattering patterns from native glycinin using different solution conditions are shown in **Figure 3a**. Scattering data from glycinin with 1 M NaI were also collected but then discarded from further analysis because of the very low signal-to-noise ratio caused by strong X-ray absorption by iodine. Apart from native glycinin, the study of another noncrystallized subunit of glycinin, A5A4B3, was investigated, and solution SAXS was collected and analyzed. The conditions used, as described in Materials and Methods, ensured the most stable hexameric subunit structure [S. Utsumi (Laboratory of Food Quality Design and Development, Graduate School of Agriculture, Kyoto University), personal communication]; however, the conditions necessary for the prevention of protein aggregation could not be achieved.

Values of R_g and D_{max} for all measured SAXS data in addition to the A1aB1b (Protein Data Bank entry 1fxz) and A3B4 (Protein Data Bank entry 1od5) subunits are summarized in **Table 1**. Since R_g and D_{max} are determined via a Fourier transform of the scattering data in inverse space (*32*, *33*), their associated errors are

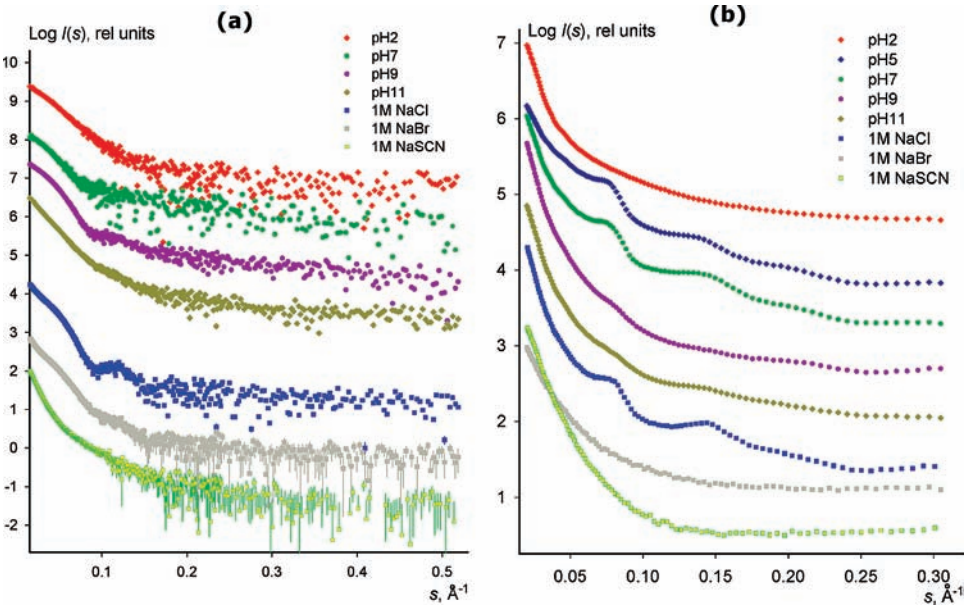

Figure 3. SAXS from (**a**) solutions and (**b**) powders of glycinin at different pH values and 1 M salt.

Table 1. Radii of Gyration (R_g) and Maximum Diameters (D_{max}) Calculated by GNOM for Experimental Data of Native Glycinin Solutions, as Well as from Protein Data Bank Structures of the Trimer and Hexamer

	c (mg/mL)	R_g (Å)	D_{max} (Å)
trimer, (1fxz)		33.3 ± 0.1	100 ± 5
trimer (1od5)		33.5 ± 0.1	100 ± 5
hexamer (1od5)		38.2 ± 0.1	105 ± 5
pH 2	3.5	42.0 ± 0.2	120 ± 8
pH 7	1.3	42.5 ± 0.2	120 ± 8
pH 9	3.0	41.8 ± 0.2	120 ± 8
pH 11	4.1	77.6 ± 0.2	250 ± 10
NaCl	2.7	42.3 ± 0.2	120 ± 8
NaBr	5.1	102.3 ± 0.2	350 ± 10
NaSCN	4.4	125.3 ± 0.2	410 ± 10

in part caused by the collection of data over a finite s range in addition to intrinsic experimental errors in the collection of data.

The R_g and D_{max} values from solutions at pH 2, 7, and 9 with 1 M NaCl are similar to each other (42 and 120 Å, respectively) and suggest that the principal components in these samples are almost identical. The pair distribution function of the pH 2 solution looks closer to that of the trimer, whereas the $p(r)$ functions for both pH 7 and 9 appear essentially identical and similar to the pattern calculated for A3B4. The $p(r)$ function for the solution with 1 M NaCl has a main peak in coincidence with those for pH 7 and 9 data sets but also produces a long shoulder that is indicative of some quantity of glycinin aggregates. The strong basic environment (pH 11) and the addition of Br^- and SCN^- generated aggregates whose shape cannot be directly related to the hexameric A3B4 shape because of insufficient additional structural information available about, for example, the relative orientation of hexameric building blocks. The ability of the salts to affect protein structure was strengthened following the order of ions in the Hofmeister series and is, in general, more significant than variations in pH over the range investigated.

Glycinin at pH 7 and 9 tends to have an overall shape close to that of the mutant hexamer A3B4. Corresponding SAXS patterns show very well-pronounced peaks at approximately the same position as those on the calculated curve from A3B4. Such a conclusion is supported by further complementary ab initio and mixture composition analysis described below. Decreasing the pH to 2 leads to protein dissociation, with the corresponding SAXS data containing no resolvable features. CD results (**Figure 2**) for pH 2 and 11 solutions are consistent with those reported by Kim et al. (*10*) and indicate that the secondary structure is largely maintained; only partial denaturation may have occurred. Kim et al. (*10*) showed that the CD spectra of soy glycinin exhibit only slight changes at different pH values and that the protein was stable at all experimental pH values studied. The CD spectra obtained in this study as well as spectra reported by Kim et al. (*10*) show a typical minimum at ~208 nm; the latter is one of the signatures of an α-helix conformation. On the basis of their assignments, pH 2 and 11 structures contain 20 and 4% α-helices and 14 and 33% β-structures, respectively.

This is similar to CD observations at the other extreme of pH 11 but with SAXS also indicating evidence for significant oligomerization [i.e., the formation of unimodal large particles, as confirmed by DLS and $p(r)$ function analysis from SAXS]. The influence of the Hofmeister ion on glycinin follows the expected behavior with $Cl^- < Br^- < SCN^-$ in terms of protein structure stability (*12*). Denaturing does not occur in the presence of NaCl, and the solution is composed of hexameric-like glycinin particles, as is the case at pH 9. NaBr has a destabilizing effect on the protein, with solution SAXS indicating the formation of particles larger than the hexamer but still well-structured. The presence of NaSCN leads to the formation of a large, ill-defined structure.

SAXS spectra for native glycinin and the corresponding $p(r)$ functions (**Figures 3a** and **4**) enabled the assessment of the similarity between the shape of the native protein and those of structures constructed from the reported subunits, namely, A1aB1b and A3B4. The radius of gyration (R_g), the maximum scattering dimension (D_{max}), and the pair distribution function [$p(r)$] for every collected data set were determined. Evidence of some aggregation can be observed, for example, as a shoulder in the NaCl $p(r)$. The experimental data clearly show the absence of concentration dependence, so subsequent analysis was conducted on data at the highest concentration available for each different solution condition. Since partial aggregation was evident in all samples, an estimate of $I(0)$ and subsequent calculation of molecular weights was not possible.

As described above, it was not possible to obtain precise shape information in solution; it was therefore not possible to directly

relate the observed scattering to the solution structure for a possible third subunit, A5A4B3. Although the structures of native glycinin trimers and hexamers are obviously not identical to those composed of A1aB1b or A3B4 subunits, they would be anticipated to be similar due to a high degree of homology in amino acid sequence of not only these two but also all five subunits. To confirm this, the scattering profiles and $p(r)$ functions from A1aB1b and A3B4 monomers and trimers were compared.

The SAXS data as well as circular dichroism confirm the observations of Kim et al. (*10*) that glycinin at pH 2 and 11 does not undergo significant denaturation. SAXS demonstrated changes to quaternary structure (hexamer dissociation and oligomerization). However, the secondary structure was preserved as CD data at pH 2 and 11 were essentially the same as those obtained at pH 9. Salt solutions were not tested due to high absorption of most salts in the far-UV region leading to signal oversaturation and a loss of sensitivity in the interpretation of CD data.

3.1.2. Construction of Glycinin Models. The overall shapes of different monomers are similar (NSD = 1.01), and the small-angle scattering patterns are similar. Trimeric A1aB1b and A3B4 show a remarkable difference in secondary and tertiary structures (**Figure 5**) but remain similar on a quaternary level (NSD = 1.01). There is no other hexameric structure available except that composed of A3B4, so the trimer A1aB1b and hexamer A3B4 are used as plausible models to compare with SAXS data from the native solutions.

All of the scattering data sets were fitted to the calculated pattern from A3B4 using CRYSOL (*34*) to determine the extent to which the solution structures are similar to the model homohexameric structure. The results indicate that scattering from the pH 7, pH 9, and 1 M NaCl solutions arises mostly from scattering of a molecule similar to A3B4. Ab initio modeling was subsequently conducted using DAMMIN (*37*) for these solutions. The structures generated (shown in **Figure 6**) clearly demonstrate that the major scattering entities at pH 7, pH 9, and 1 M NaCl are very similar to A3B4, but the samples also contain either aggregates or minor contaminants (see Sample Preparation) which give rise to an increase in the average radius of gyration and the maximum diameter of models in DAMMIN.

To estimate the amount of A3B4-like particles and the volume fractions of trimers and hexamers in solution, we used OLIGOMER (*31*). Assumptions are made that the solutions are composed exclusively of trimeric A1aB1b and hexameric A3B4 models, enabling a reasonable quantitative description of the pH 7, pH 9, and 1 M NaCl systems. It was estimated that the pH 9 solution contains approximately 12% trimeric and 88% hexameric molecules (χ = 2.35) and the 1 M NaCl solution consists mainly of hexameric species, approximately 98% (χ = 3.98). The corresponding fits are shown in **Figure 7**.

3.2. Effect of pH and Salts on Powder Structure. The observed scattering arises from a combination of Bragg diffraction from the glycinin crystal structure and the interface between the protein and the surrounding medium. The latter is responsible for the high scattering in the low-s region (Porod scattering). The data for $s < 0.057$ Å^{-1} have been fitted with a power law function (intensity $\propto s^{-p}$) with exponent "p". Scattering profiles from powdered glycinin at pH 7 and 9 as well as at extreme pH values of 2 and 11 decrease following the same power law with an exponent equal to −3.9(1). One exception from this constant behavior is the scattering intensity for the sample at pH 5 [p equal to −2.4(6)]. The exponent of approximately −4 for the samples at pH 2, 7, 9, and 11 indicates that, at a length scale of 100−300 Å

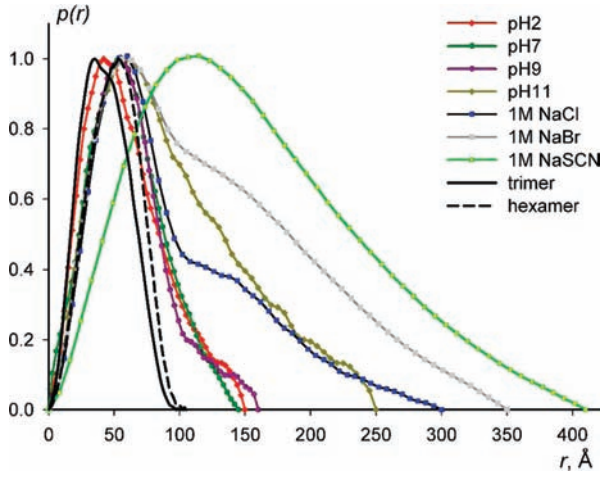

Figure 4. $p(r)$ functions obtained from calculated scattering profiles of trimer A1aB1b and hexamer A3B4 and from all experimentally collected glycinin scattering profiles.

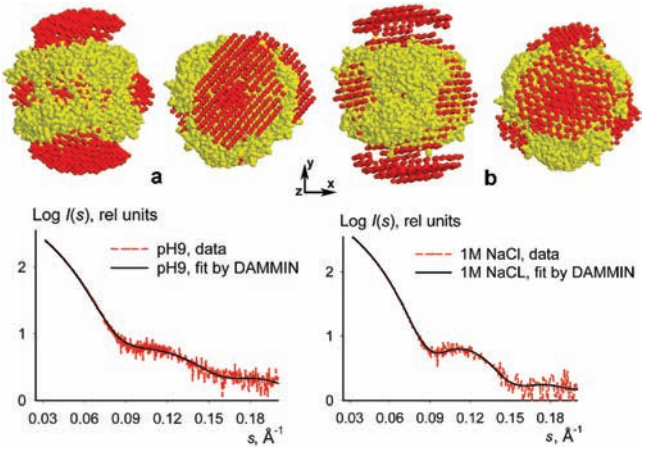

Figure 6. Models constructed by DAMMIN for scattering patterns from the pH 9 solution (left) and 1 M NaCl solution (right). The structure of the A3B4 homohexamer is colored yellow.

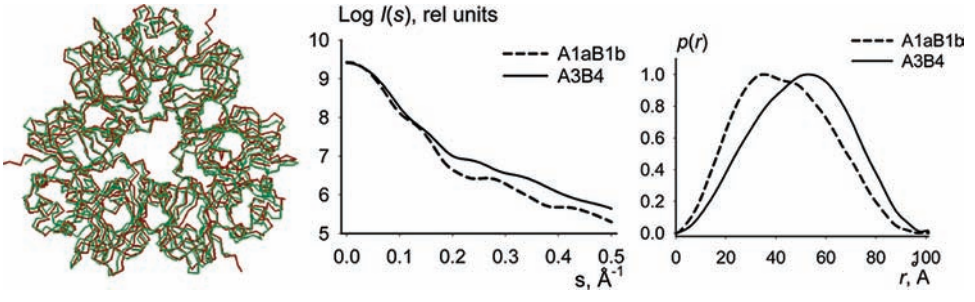

Figure 5. Trimers A1aB1b (red) and A3B4 (green) and corresponding calculated scattering intensities (middle) and $p(r)$ functions (right).

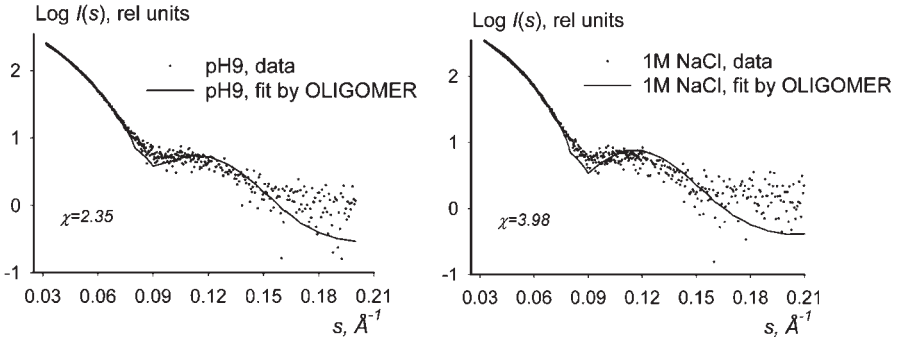

Figure 7. OLIGOMER fit of experimental patterns from the solution at pH 9 (left) and in the presence of 1 M NaCl (right) from calculated scattering from a mixture of trimers (A1aB1b) and homohexamers (A3B4).

Table 2. *s* Positions and Corresponding Real-Space Values of Resolved Peaks from Scattering Patterns from Powdered Glycinin[a]

	first peak		second peak	
	position *s* ($Å^{-1}$)	spacing *d* (Å)	position *s* ($Å^{-1}$)	spacing *d* (Å)
pH 5	0.076 ± 0.005	83 ± 6	0.137 ± 0.005	46 ± 2
pH 7	0.073 ± 0.005	86 ± 6	0.141 ± 0.005	45 ± 2
pH 9	0.078 ± 0.005	81 ± 5	0.200 ± 0.005	31 ± 1
pH 11	0.080 ± 0.005	79 ± 5	0.145 ± 0.005	43 ± 1
NaCl	0.078 ± 0.005	86 ± 6	0.144 ± 0.005	44 ± 1

[a] pH 2, NaBr, and NaSCN powders exhibit no resolvable peaks.

(where 300 Å is the maximum resolvable dimension), there is a sharp density cutoff at the solid−void interface between the protein and the surrounding medium. These exponents are similar to those observed previously on samples measured over a significantly more extended *s* range (*38*). In the latter work, this was interpreted as the interface between the "dry" protein powder and the surrounding medium being smooth and sharp over a length scale from at least 3 μm to ~20 nm. The change in slope for the pH 5 sample indicates significantly different behavior. This pH is very close to the pI of glycinin, and in this environment, the protein is relatively uncharged and partially unfolded and has an associated decrease in the energy barrier to protein−protein aggregation. It is this diffusion-limited aggregation that results in the observed fractal behavior (*39*, *40*).

The positions of the two dominant scattering peaks from the powders are summarized in **Table 2** with additional higher-angle reflections evident in **Figure 3b**. Within experimental error, our results are in accord with previous studies of Kealley et al. (*38*). In the latter, the structure of hydrated glycinin powders in the absence of salts was reported, the authors showing that Bragg peaks observed in the SAXS were consistent with a hexagonal unit cell structure with dimensions smaller than those of the mutant homohexameric protein.

As the glycinin samples were purified from pH-adjusted solutions and then freeze-dried into powder form, we expected that the solution chemistry would dominate the effects observed in the powders. Increasing the pH from neutral to pH 9 and 11 results in a dramatic loss in peak resolution; this is the result of partial unfolding of the protein which leads to a corresponding decrease in long-range order. Decreasing the pH to 2 has had a significant effect on the scattering, and no resolved structural peaks remain in the SAXS pattern. It is important to note that it is not possible here to make a direct comparison of the intensities between the powder samples, as there are possible inherent differences in packing density and, in the case of the salt series, also X-ray absorption between samples.

The powdered NaCl glycinin sample has peaks in positions similar to those of native glycinin at pH 7 and indicates that the long-range crystalline order has been maintained. The solution conditions of pH 7, pH 9, and 1 M NaCl yield a well-pronounced peak at ~0.11 $Å^{-1}$ (**Figure 3a**). The addition of 1 M NaBr initiates protein oligomerization, but a weak peak is present at the same *s* value. It is noteworthy that a similar peak appears in the calculated scattering from the A3B4 homohexamer. As expected, NaSCN has a detrimental effect on the long-range order as a result of extensive oligomerization in solution. The pH 11 and 1 M NaSCN environments result in protein oligomerization with partial denaturation in the former. At the other extreme in pH, dissociation also takes place with partial denaturation. These processes result in "featureless" SAXS patterns.

The work reported here shows that substantial findings can be obtained via application of a methodology that is typically utilized only for highly purified, single-subunit systems. Indeed, it is evident that such a formalism may be usefully applied to a real system, of industrial relevance, if appropriate assumptions are made. In this way, it has been possible to understand the main trends in glycinin structure occurring under various experimental conditions and to relate the results to the available atomic-resolution structures of A1aB1b and A3B4. It would be intriguing to develop a more detailed understanding of the powder patterns and their relationship to the corresponding solutions in these systems. This is currently limited, however, by the lack of availability of isolated and crystallized forms of all five glycinin subunits. The latter would enable atomic-resolution structures to be obtained.

Glycinin solutions and the powders from which they have been derived show pronounced characteristics of dependence in their scattering data on pH and salt in their environment. The positions of the peaks in the solvated and dry states are evidently different, but they nonetheless reflect different structural features of the individual molecules in solution and the manner of its packing in the dry samples. Scattering profiles of dry glycinin contain the signature of the extent of long-range order. The measurement of SAXS intensity from solutions under changing experimental conditions allows the possibility of monitoring conformational changes of quaternary structure of glycinin molecules. In this

way, a combination of analysis of the scattering from protein powders and solutions under matched conditions produces a broad picture of glycinin structural changes with salt and pH.

Glycinin exhibits different structural features depending on the applied external conditions. The origin of the features in the powder samples originates both from the intraparticle and interparticle effects, whereas at the concentrations used here, the features in the solutions, from which the powders have been prepared, arise primarily from intraparticle effects. Protein powders produced from solutions at pH 5 or 7 or in the presence of 1 M NaCl exhibit long-range order. In solution, native glycinin tends to form structures similar to homohexameric A3B4 under these conditions. pH 5 is close to the isoelectric point of the protein, and a precipitate results from our attempt to form a solution; the corresponding powder possesses some long-range order, but the low-q fractal behavior is consistent with cluster formation. An acidic (pH 2) environment initiates breaking of the hexameric structure into trimers, while a basic environment (pH 11) leads to the formation of large aggregates. This study showed, in accord with previous findings, that only partial denaturation occurs at extremes of pH 2 and 11, but the solution scattering indicates dissociation at the lower pH and oligomerization at the higher pH. The small scattering peak in the pH 11 powder illustrates a reduced correlation length, whereas dissociation in the solution leads to featureless scattering in the powder at pH 2. The scattering pattern from a 1 M NaBr solution shows peaks at the same scattering angle $\{s \sim 0.115\ \text{Å}^{-1}\ [d = 54.6(4)\ \text{Å}]\}$ as 1 M NaCl data and compares favorably with the scattering profile calculated for hexameric A3B4; this indicates significant structural similarity. However, there is evidence of the formation of particles 3−4 times larger than hexamers in the latter solution, and this is likely to result in a reduction in long-range order observed in the corresponding powder. The strongest denaturing condition, i.e., 1 M NaSCN, caused oligomerization of glycinin molecules both in solution and in the corresponding powder states.

An understanding of such protein structural changes under various environmental conditions, and the extent of structure modifications as a result of drying, will enable the development of ingredients and food formulations with increased stability, longer shelf life, and improved sensory properties. A deep understanding of the behavior of a real and ubiquitous food protein, namely soy glycinin, was achieved through the simultaneous analysis of a series of scattering data under the same conditions in solution and in the dry state. While we were unable to determine the path of glycinin structural changes during drying from the protein solution to form the powder, the behavior of the protein has been analyzed over a broad range of environmental conditions of pH and salt content. Our future interests are to investigate kinetically how the protein structure changes as a function of increasing concentration as the system passes from a dilute solution to a concentrated powder. A sophisticated analysis of the solution SAXS has not been possible in this study due to the non-model nature of the protein. However, we intend to apply the methodology of Zhang et al. (*21*) as applied to BSA to enable a more detailed determination of the solution and freeze-dried nanostructures of the same model protein. Such an approach would be most successful in a study of the mutant homohexameric form of the protein. Nonetheless, we have shown for the first time the influence of pH and salt on the structure of freeze-dried protein powders and their correlation with solutions from which they have been formed. This methodology is likely to prove invaluable not only to the food industry but also to researchers working in broad fields of protein-oriented applications.

ACKNOWLEDGMENT

This work was conducted in collaboration with the CSIRO Food Futures Flagship, Food Science Australia. We thank Dr. Ingrid Appleqvist, Dr. Manoj Rout, and the team at Food Science Australia in North Ryde, NSW, Australia, for providing the glycinin samples and valuable discussions. We appreciate Professor S. Utsumi of the Laboratory of Food Quality Design and Development at the Graduate School of Agriculture at Kyoto University for providing the A5A4B3 subunit sample for study, the Biological small-angle scattering group for providing the synchrotron research facilities used in this work, and the help of Dr. Maxim Petoukhov during SAXS data collection. We would also like to thank Dr. Dmitri Svergun at EMBL for suggesting this approach. CD and DLS spectrometers located at the National Deuteration Facility (ANSTO) were partly funded by the National Collaborative Research Infrastructure Strategy of the Australian Government.

LITERATURE CITED

(1) Michelfelder, A. J.*Am. Fam. Physician* **2009**, *79*, 43–47.
(2) Choi, S.; Adachi, M.; Yoshikawa, M.; Maruyama, N.; Utsumi, S. *Biosci., Biotechnol., Biochem.* **2004**, *68*, 1991–1994.
(3) Badley, R. A.; Atkinson, D.; Hauser, H.; Oldani, D.; Green, J. P.; Stubb, J. M.*Biochim. Biophys. Acta* **1975**, *412* (2), 214–228.
(4) Koshiyama, I.*Int. J. Pept. Protein Res.* **1972**, *4* (3), 167–176.
(5) Kitamura, K.; Takagi, T.; Shibasaki, K.*Agric. Biol. Chem.* **1976**, *9*, 1837–1844.
(6) Adachi, M.; Kanamori, J.; Masuda, T.; Yagasaki, K.; Kitamura, K.; Mikami, B.; Utsumi, S.*Proc. Natl. Acad. Sci. U.S.A.* **2003**, *100* (12), 7395–7400.
(7) Adachi, M.; Takenaka, Y.; Gidamis, A. B.; Mikamu, B.; Utsumi, S. *J. Mol. Biol.* **2001**, *305* (2), 291–305.
(8) Lakemond, C. M.; de Jongh, H. H.; Hessing, M.; Gruppen, H.; Voragen, A. G.*J. Agric. Food Chem.* **2000**, *48* (6), 1985–1990.
(9) Lakemond, C. M.; de Jongh, H. H.; Hessing, M.; Gruppen, H.; Voragen, A. G.*J. Agric. Food Chem.* **2000**, *48* (6), 1991–1995.
(10) Kim, K. S.; Kim, S.; Yang, H. J.; Kwon, D. Y.*Int. J. Food Sci. Technol.* **2004**, *39*, 385–393.
(11) Koshiyama, I.*J. Sci. Food Agric.* **1972**, *23*, 853–869.
(12) Hofmeister, F.*Arch. Exp. Pathol. Pharmakol.* **1888**, *24*, 247–260.
(13) Hribar, B.; Southall, N. T.; Vlacy, V.; Dill, K. A.*J. Am. Chem. Soc.* **2002**, *124*, 12302–12311.
(14) Zou, Q.; Bennion, B. J.; Daggett, V.; Murphy, K. P.*J. Am. Chem. Soc.* **2002**, *124*, 1192–1202.
(15) Batchelor, J. D.; Olteanu, A.; Tripathy, A.; Pielak, G. J.*J. Am. Chem. Soc.* **2004**, *126*, 1958–1961.
(16) Omta, A. W.; Kropman, M. F.; Woutersen, S.; Bakker, H. J.*Science* **2003**, *301*, 347–349.
(17) Zhang, Y.; Cremer, P. S.*Curr. Opin. Chem. Biol.* **2006**, *10*, 658–663.
(18) Baldwin, R. L.*Biophys. J.* **1996**, *71*, 2056–2063.
(19) Babajimopoulos, M.; Damodaran, S.; Rizvi, S. S. H.; Kinsella, J. E. *J. Agric. Food Chem.* **1983**, *31* (6), 1270–1275.
(20) Damodaran, S.*J. Agric. Food Chem.* **1988**, *36* (2), 262–269.
(21) Zhang, F.; Skoda, M. W. A.; Jacobs, M. J.; Martin, R. A.; Martin, C. M.; Schreiber, F.*J. Phys. Chem. B* **2007**, *111*, 251–259.
(22) Kealley, C. R.; Rout, M. K.; Dezfouli, M. R.; Strounina, E.; Whittaker, A. K.; Appelqvist, I. A. M.; Lillford, P. J.; Gilbert, E. P.; Gidley, M. J.*Biomacromolecules* **2008**, *9* (10), 2937–2946.
(23) Bogracheva, T. Ya.; Leont'ev, N. Y.*Appl. Biochem. Microbiol.* **1996**, *32* (4), 429–433.
(24) Gasteiger, E.; Gattiker, A.; Hoogland, C.; Ivanyi, I.; Appel, R. D.; Bairoch, A.*Nucleic Acids Res.* **2003**, *31*, 3784–3788.
(25) Garcia de la Torre, J. G.; Navarro, S.; Lopez Martinez, M. C.; Diaz, F. G.; Lopez Cascales, J.*Biophys. J.* **1994**, *67*, 530–531.
(26) Garcia de la Torre, J. G.; Huertas, M. L.; Carrasco, B.*Biophys. J.* **2000**, *78*, 719–730.
(27) Garcia de la Torre, J. G.; Carrasco, B.*Biopolymers* **2002**, *63*, 163–167.

(28) Nagano, T.; Mori, H.; Nishinari, K.*J. Agric. Food Chem*. **1994**, *42* (7), 1415–1419.
(29) Whitmore, L.; Wallace, B. A.*Nucleic Acids Res*. **2004**, *32*, W668–W673.
(30) Konarev, P. V.; Volkov, V. V.; Sokolova, A. V.; Koch, M. H. J.; Svergun, D. I.*J. Appl. Crystallogr*. **2003**, *36*, 1277–1282.
(31) Konarev, P. V.; Petoukhov, M. V.; Volkov, V. V.; Svergun, D. I. *J. Appl. Crystallogr*. **2006**, *39*, 277–286.
(32) Svergun, D. I.; Semenyuk, A. V.; Feigin, L. A.*Acta Crystallogr*. **1988**, *A44*, 244–250.
(33) Svergun, D. I.*J. Appl. Crystallogr*. **1992**, *25*, 495–503.
(34) Svergun, D. I.; Barberato, C.; Koch, M. H. J.*J. Appl. Crystallogr*. **1995**, *28*, 768–773.
(35) Kozin, M. B.; Svergun, D. I.*J. Appl. Crystallogr*. **2001**, *34*, 33–41.
(36) Ilavsky, J. Advanced Photon Source, Chicago, 2006.
(37) Svergun, D. I.*Biophys. J*. **1999**, *76*, 2879–2886.
(38) Kealley, C. E.; Elcombe, M. M.; Wuhrer, R.; Gilbert, E. P.*J. Appl. Crystallogr*. **2008**, *41*, 628–633.
(39) Schaefer, D. W.; Martin, J. E.; Wiltzius, P.; Cannell, D. S.*Phys. Rev. Lett*. **1984**, *52*, 2371–2374.
(40) Maurice, K.; Lavrentovich, O. D. Soft Matter Physics: An Introduction. In *Fractals and Growth Phenomena*; Springer: Dordrecht, The Netherlands, 2003.

Received for review July 9, 2009. Revised manuscript received October 29, 2009. Accepted November 17, 2009. We acknowledge travel grants through the Access to Major Research Facilities Programme which is a component of the International Science Linkages Programme established under the Australian Government's innovation statement, Backing Australia's Ability. We also acknowledge the support of the European Molecular Biology Laboratory, c/o DESY, Hamburg, Germany.